

## Experimental and Theoretical Study of the Structure and Reactivity of $\text{Fe}_{1-2}\text{O}_{\leq 6}^-$ Clusters with CO

Nelly M. Reilly,<sup>†</sup> J. Ulises Reveles,<sup>‡</sup> Grant E. Johnson,<sup>†</sup> Shiv N. Khanna,<sup>‡</sup> and A. W. Castleman, Jr.\*<sup>†</sup>

Departments of Chemistry and Physics, Pennsylvania State University, University Park, Pennsylvania 16802, and Department of Physics, Virginia Commonwealth University, Richmond, Virginia 23234

Received: January 9, 2007; In Final Form: February 16, 2007

Synergistic studies employing experiments in the gas phase and theoretical first principles calculations have been carried out to investigate the structure, stability, and reactivity toward CO of iron oxide cluster anions,  $\text{Fe}_x\text{O}_y^-$  ( $x = 1-2$ ,  $y \leq 6$ ). Collision-induced dissociation studies of iron oxide species, employing xenon collision gas, show that  $\text{FeO}_3^-$  and  $\text{FeO}_2^-$  are the stable building blocks of the larger iron oxide clusters. Theoretical calculations show that the fragmentation patterns leading to the production of O or  $\text{FeO}_n$  fragments are governed both by the energetics of the overall process as well as the number of intermediate states and the changes in spin multiplicity. Mass-selected experiments identified oxygen atom transfer to CO as the dominant reaction pathway for most anionic iron oxide clusters. A theoretical analysis of the molecular level pathways has been carried out to highlight the role of energetics as well as the spin states of the intermediates on the oxidation reaction.

### Introduction

Transition metal catalysts, specifically those composed of iron nanoparticles, have been employed in many industrial and biological processes as well as pollution abatement applications.<sup>1</sup> Lin et al. observed nanosized iron oxides to be highly active for CO oxidation at low temperatures.<sup>2</sup> In addition to other studies probing the oxidation of carbon monoxide with iron,<sup>3</sup> iron oxides showed activity for the oxidation of methane<sup>4</sup> and various hydrocarbons.<sup>5</sup> Iron oxides are also promising because they exhibit good catalytic lifetimes and resistance to high concentrations of moisture and  $\text{CO}_2$ , which often poison catalysts.<sup>6</sup> Therefore, iron oxides may become economical alternatives to costly precious metal catalysts.

Studies involving iron and iron oxide have been conducted previously through both calculations<sup>7-9</sup> and photoelectron spectroscopy experiments.<sup>10-12</sup>  $\text{FeO}$ ,  $\text{Fe}_2\text{O}_3$ , and  $\text{Fe}_3\text{O}_4$  are stable stoichiometries in the condensed phase; thus, they are the most studied species.<sup>10,13</sup> It was suggested by Li and co-workers that  $\text{Fe}_2\text{O}_3$  was the most active species for oxidation, showing that  $\text{Fe}_2\text{O}_3$  behaved as a catalyst in the presence of  $\text{O}_2$  and as a reagent in the absence of oxygen, oxidizing CO to  $\text{CO}_2$ .<sup>13</sup> Sequential reduction of  $\text{Fe}_2\text{O}_3$  in the absence of  $\text{O}_2$  produced  $\text{Fe}_3\text{O}_4$ ,  $\text{FeO}$ , and  $\text{Fe}$  species. Previous calculations of the reaction of neutral  $\text{Fe}_2\text{O}_3$  with CO led to a proposed mechanism with a viable energetic pathway to produce  $\text{CO}_2$ .<sup>14-16</sup> Through cooperative effects, the adsorption of CO onto the cluster was predicted to weaken a Fe–O bond and made this oxygen readily available to a second CO for easy formation of  $\text{CO}_2$ .

Iron oxide layers are commonly employed in catalytic supports and have shown active participation in the reactions.<sup>6,17</sup> Iron is unique and more active than other supports because it is

easily reduced and allows anion vacancy formation due to a highly disordered structure.<sup>18,19</sup> Anion vacancies are important in the catalytic process because they stabilize the supported clusters and influence charge density. Schubert et al. studied several different transition metal supports and found that iron oxides were able to adsorb large amounts of oxygen.<sup>17</sup> In addition to the adsorbed oxygen participating in the process, they proposed a mechanism that allowed for the oxide support to supply the oxygen for the reaction. The ability of iron oxide to function both ways greatly enhanced the oxidation activity.

Gas-phase cluster studies are especially amenable to elucidating the structure and active sites of reactive species. These studies eliminate the uncertainty of different catalyst preparation methods and allow for fundamental insight into site specific activity. Clusters, therefore, are ideal models to identify what occurs on a catalytic surface and to help elucidate molecular level reaction mechanisms. Numerous studies have shown similar products from reactions of metal oxides in both the condensed and gas phase.<sup>20-24</sup> Our present joint experimental and theoretical study aids in uncovering species with increased activity and selectivity for the oxidation of CO to  $\text{CO}_2$ . The results provide important insight into the nature of the active sites responsible for condensed phase catalysis, shedding light on the role of cluster size, charge and oxidation state, composition, and stoichiometry toward CO oxidation in the presence of iron oxide. We focus on anionic iron oxide behavior herein, and address charge state and electron density effects on the structure and bonding of small cationic iron oxide clusters in a separate publication.<sup>25</sup>

### Experimental Methods

Gas-phase cluster studies were performed using a guided ion beam mass spectrometer coupled to a laser vaporization source, explained in detail previously.<sup>26</sup> Briefly, the second harmonic of a Nd:YAG laser was used to ablate a rotating and translating iron rod (PVD Materials Corp., 99.95% purity). At a predeter-

\* To whom correspondence should be addressed. Tel: (814) 865 7242. Fax: (814) 865 5235. E-mail: awc@psu.edu.

<sup>†</sup> Pennsylvania State University.

<sup>‡</sup> Virginia Commonwealth University.

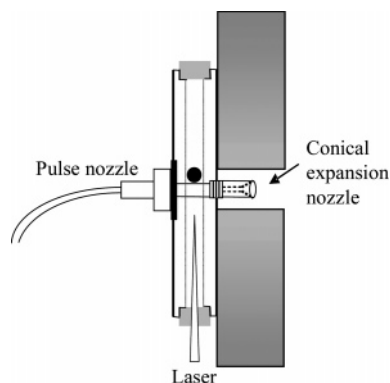


**Figure 1.** Laser vaporization source showing conical expansion nozzle screwed into the exit channel.

mined time, oxygen seeded in helium (~1%) was pulsed over the rod, forming a dense, hot plasma. A 27 millimeter (mm) conical expansion nozzle was placed at the exit of the source, shown schematically in Figure 1, allowing for more third-body collisions and aiding in larger cluster formation. The nozzle was composed of a 15 mm long channel with a 4 mm diameter and 12 mm conical expansion cone with a 30° total internal angle. The clusters then underwent supersonic expansion in a field free region before passing through a 3 mm skimmer which created a molecular beam. The cooled clusters were then focused by a set of electrostatic lenses and deflectors into the first quadrupole mass filter. Each cluster species was individually selected in the first quadrupole and directed through a second set of lenses into the octopole reaction cell. Carbon monoxide reactant gas, ranging from 0 to 20 mTorr, was added to the reaction cell and the pressure was monitored by a MKS baratron. The products were focused by a third set of lenses into the second quadrupole where they were mass analyzed and finally detected using a channel electron multiplier. Studies were also conducted with nitrogen in the reaction cell under the same conditions of pressure and energy for verification of a chemical reaction with carbon monoxide. Since both CO and N<sub>2</sub> are of the same nominal mass, experiments with N<sub>2</sub> aided in identifying collisional fragmentation products. Collision-induced dissociation (CID) experiments were conducted to study the fragmentation patterns of the iron oxide clusters. In these experiments, inert xenon gas was introduced into the reaction cell under single collision conditions (0.09 mTorr) while the kinetic energy of the ions in the octopole reaction cell was slowly raised from 0 to 40 eV laboratory frame energy. Experiments with slightly higher collision pressures, 0.2 mTorr of Xe, were conducted to find sequential fragmentation patterns under multiple collision conditions.

### Theoretical Methods

The theoretical studies were carried out using two different numerical schemes that were developed within a density functional formalism.<sup>27</sup> The exchange and correlation effects were incorporated through the generalized gradient approximation (GGA) via a functional proposed by Perdew, Burke, and Ernzerhof.<sup>28</sup> The electronic structure was determined using a linear combination of atomic orbitals molecular orbital approach. The wave function for the cluster was constructed by a linear combination of Gaussian type orbitals centered at the atomic positions in the cluster. The actual calculations employed two different numerical programs. Most calculations were carried out using the Naval Research Laboratory Molecular Orbital Library (NRLMOL) set of codes developed by Pederson and

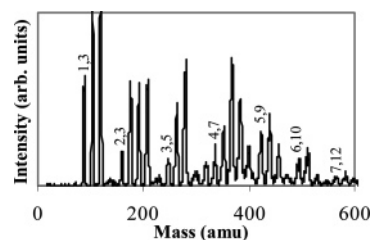


**Figure 2.** A typical mass distribution produced for iron oxide anionic clusters. The first iron oxide in each series is labeled according to Fe<sub>x</sub>O<sub>y</sub><sup>-</sup>, where (x,y) with subsequent peaks in the series have one additional oxygen atom.

co-workers.<sup>29-31</sup> For these calculations, we employed a 5s, 4p, and 3d basis set for the C and O atoms and 7s, 5p, and 4d basis for the Fe atom.<sup>31</sup> In each case, the basis set was supplemented by a diffuse Gaussian. For more details, the reader is referred to the original papers.<sup>29-31</sup> Supplementary calculations were also carried out using the deMon2K software<sup>32</sup> in order to eliminate any uncertainties associated with the choice of basis set or the numerical procedure. In these studies, we employed a gradient-corrected density functional<sup>28</sup> and the double- $\zeta$  valence polarized (DZVP) basis sets<sup>33</sup> for C and O and the Wachters-F basis set<sup>34</sup> for Fe. The GEN-A2 auxiliary function set for C and O and the GEN-A2\* auxiliary function set for Fe were used. For each cluster structure, the configuration space was sampled by starting from several initial configurations. Then the geometry was optimized by moving the atoms in the direction of the forces until they dropped below a threshold value. Since transition metal atoms are marked by nonzero spin multiplicities, the calculations included optimizing the spin multiplicities of each cluster.

### Results and Discussion

The anionic iron oxide cluster distribution with both dissociated and molecular oxygen adsorbed at near thermal energy is shown in Figure 2. Expansion gas mixtures ranging from 1–20% oxygen were investigated, with the lowest percentage of oxygen in helium providing the broadest cluster distribution. Various conditions at the exit of the source were also examined and experiments conducted with no conical expansion nozzle produced only monomer iron oxide species. A conical nozzle placed at the end of the source region before the field free expansion region (see Figure 1) allowed for more collisions and thus better iron oxide clustering. A 27 mm nozzle was used because the longer nozzle (51 mm) produced species that were more oxygen rich possessing large numbers of molecularly bound O<sub>2</sub> units. We did not generate any stoichiometric Fe<sub>x</sub>O<sub>y</sub><sup>-</sup> clusters with  $x = y$  having the same number of iron and oxygen atoms. It is interesting to note that Bernstein and co-workers produced neutral iron oxide clusters with oxygen deficient stoichiometries by varying the oxygen concentration in the system.<sup>35</sup> They made oxygen deficient iron oxide clusters employing a 0.1% oxygen mixture. However, in our source this concentration produced a narrower mass distribution of iron oxide clusters than the 1% oxygen mixture. The following studies include FeO<sub>2-4</sub><sup>-</sup> and Fe<sub>2</sub>O<sub>3-6</sub><sup>-</sup> anionic species, mostly with an oxygen-rich metal to oxygen ratio of  $x/y < 1$ .

**Structures.** Figure 3 shows the calculated optimized lowest-energy structures for the FeO<sub>1-4</sub><sup>-</sup> and Fe<sub>2</sub>O<sub>2-6</sub><sup>-</sup> clusters. For iron oxide clusters containing a single Fe atom, oxygen atoms bind directly to the metal with no molecular oxygen units. The maximum coordination number of Fe was four in the tetrahedral form of FeO<sub>4</sub><sup>-</sup>. For FeO<sub>5</sub><sup>-</sup> (not shown), the fifth oxygen attaches

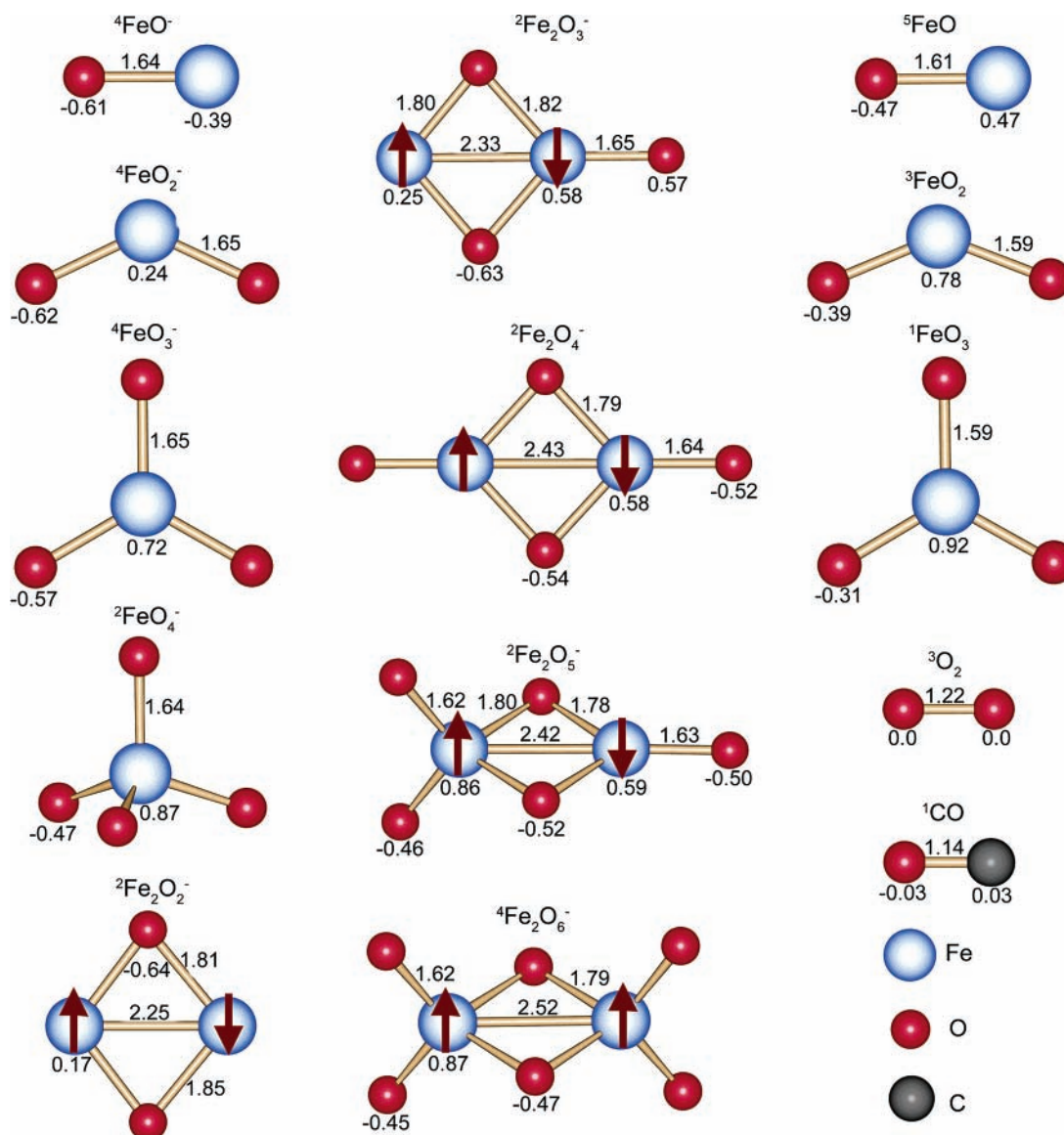


**Figure 3.** The ground state geometries of  $\text{O}_2$ ,  $\text{CO}$ ,  $\text{FeO}_{1-3}$ , and  $\text{Fe}_x\text{O}_y^-$  clusters. The bond lengths are given in Angstroms and the superscripts indicate the spin multiplicity. The arrows indicate the spin polarization at the Fe atoms for the  $\text{Fe}_2\text{O}_y^-$  clusters. The Mulliken charges are marked below each atom.

to an oxygen atom forming an  $\text{O}_2$  unit. In the case of  $\text{FeO}_6^-$  (not shown), a  $\text{FeO}_4^-$  unit with a  $\text{O}_2$  molecule is bound to an oxygen atom at a distance of 3.1 Å. A higher-energy isomer for  $\text{FeO}_4^-$  possessing a molecular oxygen subunit was 0.78 eV above ground-state energy. The Fe–O bond lengths for  $\text{FeO}_{1-4}^-$  are relatively similar. The spin multiplicity changes from quartet in  $\text{FeO}_{1-3}^-$  species to doublet for  $\text{FeO}_4^-$ .

In the iron oxide clusters containing two Fe atoms, a basic ring structure composed of  $\text{Fe}_2\text{O}_2^-$  with oxygen bridging each iron atom is formed.  $\text{Fe}_2\text{O}_3^-$  and  $\text{Fe}_2\text{O}_4^-$  have their third and fourth oxygen atoms attached to iron outside the ring. The addition of oxygen atoms to the cluster shortens the Fe–O bond length from 1.85 to 1.79 Å within the ring and 1.65 to 1.62 Å outside. Maximum coordination was obtained for the  $\text{Fe}_2\text{O}_6^-$  cluster with two extra oxygen atoms bound directly to each Fe atom. A higher-energy isomer of  $\text{Fe}_2\text{O}_6^-$  with an  $\text{O}_2$  subunit was found 1.23 eV above the ground state. An anti-ferromagnetic spin coupling was found for  $\text{Fe}_2\text{O}_2^-$ ,  $\text{Fe}_2\text{O}_3^-$ ,  $\text{Fe}_2\text{O}_4^-$ , and  $\text{Fe}_2\text{O}_5^-$  cluster species. However, the Fe sites in  $\text{Fe}_2\text{O}_6^-$  were found to be coupled ferromagnetically. Similar progressions of the exchange coupling with oxidation have been reported for the case of  $\text{Cr}_2\text{O}_n$  clusters.<sup>36</sup>

**CID Fragmentation.** Collision induced dissociation studies were undertaken with inert xenon gas under single (0.09 mTorr) and multiple (0.2 mTorr) collision conditions and the results are listed in Table 1. The fragmentation of selected clusters and their corresponding neutral loss aids in elucidating the structures of charged clusters and obtaining the general order of bond strength. Trends have been established between the calculated dissociation energies (DE) and the order of experimental fragmentation products, which are discussed below.

For  $\text{FeO}_n^-$  clusters containing a single Fe atom, the observed fragmentation channels with Xe correspond to the loss of an O atom or  $\text{O}_2$  molecule. For  $\text{FeO}_2^-$  and  $\text{FeO}_3^-$ , the pathway at the lowest energy corresponds to the loss of an atomic O, while for  $\text{FeO}_4^-$ , the loss of  $\text{O}_2$  is the lowest-energy pathway. At higher collision energies,  $\text{FeO}_4^-$  does lose an O atom. More interesting are the fragmentation channels for  $\text{Fe}_2\text{O}_n^-$  clusters containing two Fe atoms. In the case of  $\text{Fe}_2\text{O}_3^-$ , the product channel that is observed at the lowest collision energy is loss of an O atom. In contrast, the product channel that is observed at the lowest collision energy for  $\text{Fe}_2\text{O}_4^-$  is loss of FeO. In the case of  $\text{Fe}_2\text{O}_5^-$ , the lowest-energy channel involves the loss of a  $\text{FeO}_2$ , while for  $\text{Fe}_2\text{O}_6^-$ , the loss of an  $\text{O}_2$  molecule is the

**TABLE 1: The Collision Induced Dissociation Fragmentation Channels, Calculated Dissociation Energies (DE), and Reaction Products with CO and N<sub>2</sub> for Fe<sub>1,2</sub>O<sub>2-6</sub><sup>-</sup> Clusters**

Fe <sub>x</sub> O <sub>y</sub> <sup>-</sup> (x, y)	products with Xe <sup>a</sup>	neutral(s) lost <sup>b</sup>	DE (eV)	products with CO	products with N <sub>2</sub>
1, 2	1, 1	0, 1	6.03	1, 1	no products
1, 3	1, 2	0, 1	5.8	1, 2	no products
1, 4	1, 2	0, 2	3.47	1, 2	1, 2 <sup>c</sup>
2, 3	1, 3	0, 1	3.87	1, 3 <sup>c</sup>	
	2, 2	0, 1	6.10	2, 2	no products
	1, 2	1, 1	3.70		
2, 4	1, 3	1, 0	3.41		
	1, 3	1, 1	3.94	2, 3	no products
	1, 2	1, 2	4.68	1, 3	
2, 5	2, 3	0, 1	6.03		
	1, 3	1, 2	3.44	2, 4	no products
	2, 4	0, 1	4.56	1, 3	
2, 6	2, 3	0, 2 <sup>c</sup>	4.39		
	2, 4	0, 2 <sup>d</sup>	2.90	2, 4	2, 4 ≈ 2, 5 <sup>c</sup>
	2, 5	0, 1	4.55	2, 5 <sup>c</sup>	
	1, 3	1, 3 <sup>c</sup>	3.22		

<sup>a</sup> Fragmentation channels are shown in order of observation with increasing collision energy. <sup>b</sup> Neutral loss is assigned based on the difference between the selected cluster and fragment ion formed. <sup>c</sup> Channels taking place under multiple collision conditions. <sup>d</sup> Dissociation occurs at near thermal energies.

lowest-energy channel. In each case, other channels do open up as the energy is increased. The basic question is then whether the onset of these pathways may be explained by the energetics of fragmentation.

To answer this question, we calculated the energies required to remove an O, O<sub>2</sub>, O<sup>-</sup>, and O<sub>2</sub><sup>-</sup> from FeO<sub>n</sub><sup>-</sup> and Fe<sub>2</sub>O<sub>n</sub><sup>-</sup> clusters and the energies for fragmentation pathways leading to the production of Fe, FeO, FeO<sub>2</sub>, and FeO<sub>3</sub> in the case of Fe<sub>2</sub>O<sub>n</sub><sup>-</sup> clusters. The results of these investigations are plotted in Figure 4 and the exact values are provided in the supplemental Tables S1, S2, S3, S4, and S5. The calculated dissociation energies for various reaction channels corresponding to observed experimental products are recorded in Table 1. We first discuss the trends in the theoretical results in Figure 4.

Since the current experiments detect anionic species, only the loss of neutral O and O<sub>2</sub> subtracted from the mass selected cluster can be experimentally observed. For FeO<sub>n</sub><sup>-</sup> clusters, one notices that the energy to remove an O atom or an O<sub>2</sub> molecule decreases with increasing oxygen coverage. As an example, while it takes 5.99 eV to remove an O atom from FeO<sub>2</sub><sup>-</sup>, only 3.86 eV is needed to remove an O atom from FeO<sub>4</sub><sup>-</sup>. This decrease makes the removal of O<sub>2</sub> a favorable channel at higher oxygen coverage particularly since energy may be gained when two O atoms combine to form an O<sub>2</sub> molecule. Indeed, for FeO<sub>4</sub><sup>-</sup>, the energy to remove an O<sub>2</sub> molecule is noticeably less than to remove an O atom, while for FeO<sub>5</sub><sup>-</sup>, it will take only 0.95 eV to remove an O<sub>2</sub> molecule. This is generally consistent with the observed fragmentation patterns in Table 1, which shows the loss of O as the preferred pathway for FeO<sub>2</sub><sup>-</sup> and FeO<sub>3</sub><sup>-</sup>, while the lowest pathway for FeO<sub>4</sub><sup>-</sup> fragmentation is the loss of an O<sub>2</sub> molecule.

For Fe<sub>2</sub>O<sub>n</sub><sup>-</sup> clusters, the fragmentation pathways include the production of Fe, FeO, FeO<sub>2</sub> and possibly FeO<sub>3</sub> fragments. The dissociation energies are shown graphically in Figure 4; the exact values are provided in a supplemental Table S1. The dissociation energy values associated with experimental products are also recorded in Table 1. It is interesting to note that the loss of O<sub>2</sub> reaches an energetic minimum for Fe<sub>2</sub>O<sub>6</sub><sup>-</sup> as the energy needed to break two Fe–O bonds is likely to be overcome by the exothermic formation of O<sub>2</sub> releasing 6.21 eV of energy. Oxygen

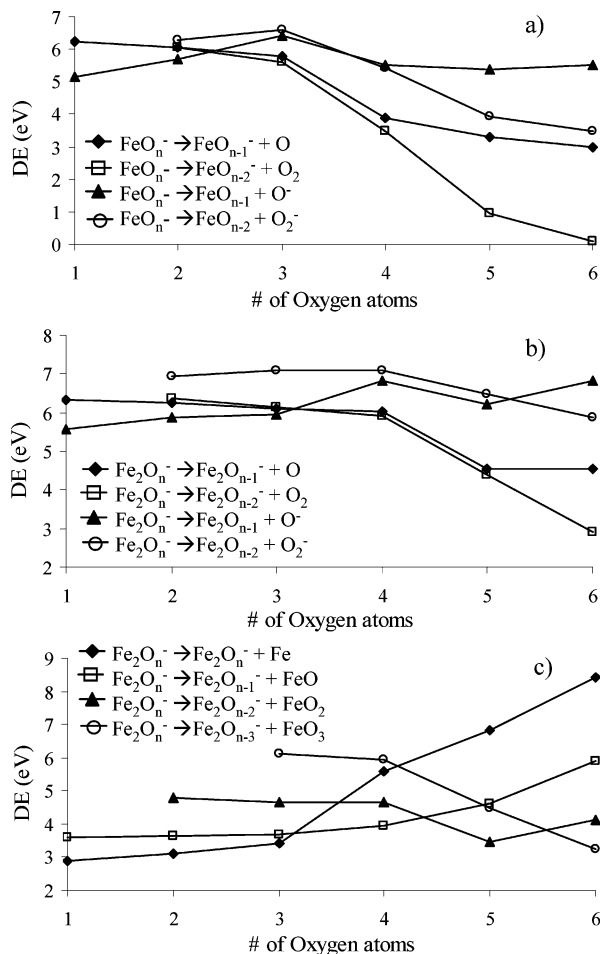


**Figure 4.** Graphs of the dissociation energy associated with removing an O atom or O<sub>2</sub> subunit from (a) FeO<sub>n</sub><sup>-</sup> and (b) Fe<sub>2</sub>O<sub>n</sub><sup>-</sup>. (c) Graph of the dissociation energy associated with removing Fe or FeO<sub>n</sub> from Fe<sub>2</sub>O<sub>n</sub><sup>-</sup> clusters.

recombination was also observed in CID studies previously conducted in our laboratory with V<sub>2</sub>O<sub>5</sub><sup>+</sup>.<sup>37</sup> The structure of V<sub>2</sub>O<sub>5</sub><sup>+</sup> contained only atomic oxygen bonds to the metal;<sup>38</sup> however, dissociation of O<sub>2</sub> was observed.

Breaking of Fe–Fe bonds occurred in the dimer clusters, mostly at higher energies or under multiple collision conditions. The core structure of the dimer clusters after fragmentation was either FeO<sub>3</sub><sup>-</sup> or FeO<sub>2</sub><sup>-</sup>, which represent the stable building blocks of the larger iron oxide clusters. Fragmentation of neutral FeO from the Fe<sub>2</sub>O<sub>4</sub><sup>-</sup> cluster requires 3.94 eV of overall energy as shown in Figure 5 that depicts various steps in the dissociation process. The dissociation of Fe<sub>2</sub>O<sub>4</sub><sup>-</sup> begins with the breaking of the bond between an Fe atom and a bridging O atom, which changes its coordination to become a terminal O atom, requiring 0.81 eV. Breaking the Fe–Fe bond and internal rotation of an FeO<sub>2</sub> subunit then leads to a chain structure and requires an additional 0.29 eV. From this open structure, it takes an additional 2.84 eV to lose neutral FeO and 3.59 eV to lose FeO<sub>2</sub>. The fragmentation of neutral FeO<sub>2</sub> from Fe<sub>2</sub>O<sub>5</sub><sup>-</sup>, shown in Figure 6, only requires 2.83 eV after structural rearrangement. Figure 4 shows that more energy is needed to fragment neutral FeO<sub>2</sub> from Fe<sub>2</sub>O<sub>4</sub><sup>-</sup> than neutral FeO; however, this order is reversed in the case of Fe<sub>2</sub>O<sub>5</sub><sup>-</sup>. Therefore our theoretical results verify the experiments that show dissociation of FeO from Fe<sub>2</sub>O<sub>4</sub><sup>-</sup> is observed at lower energy while fragmentation of FeO<sub>2</sub> required additional energy. These two clusters are unique because they form the stable fragment FeO<sub>3</sub><sup>-</sup> prior to oxygen loss. This indicates that the Fe–O bonds for Fe<sub>2</sub>O<sub>4</sub><sup>-</sup> and Fe<sub>2</sub>O<sub>5</sub><sup>-</sup>

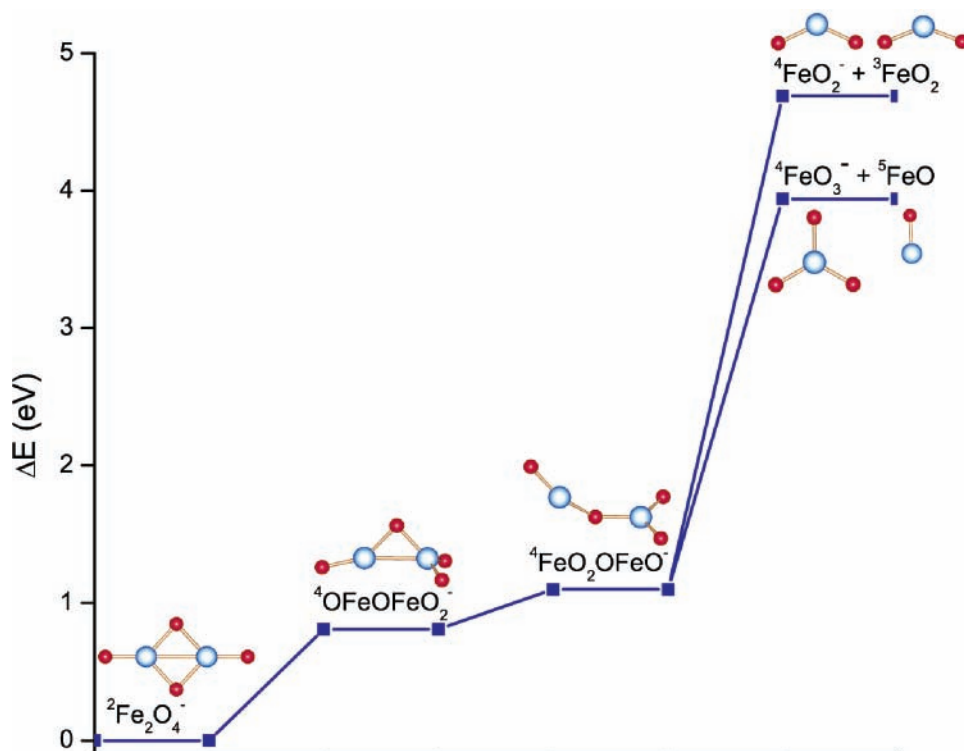


**Figure 5.** The change in energy ( $\Delta E$ ) for the dissociation pathway of  $\text{Fe}_2\text{O}_4^-$  to  $\text{FeO}_3^-$  and  $\text{FeO}_2^-$ . The superscripts indicate the spin multiplicity.

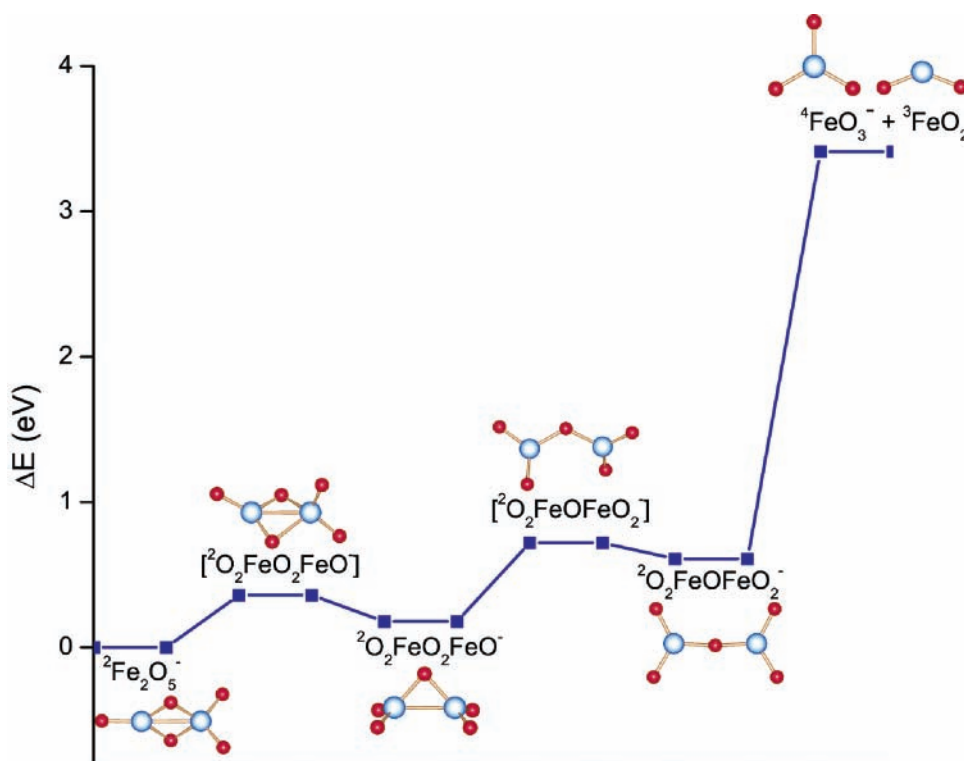


**Figure 6.** The change in energy ( $\Delta E$ ) for the dissociation pathway of  $\text{Fe}_2\text{O}_5^-$  to  $\text{FeO}_3^-$ . The superscripts indicate the spin multiplicity.

are very strong. Indeed, it requires 6.03 and 4.56 eV to break the Fe–O bonds, respectively.

In the case of  $\text{Fe}_2\text{O}_3^-$ , loss of an oxygen atom is the first observed fragment. This fragment does not follow the pattern of dissociation energies listed in Table 1. Figure 7 shows the change in energy for the dissociation pathways for neutral Fe and FeO loss. Supplemental Table S4 shows the corresponding energies for each reaction step associated with the two possible bond fragmentations. In both pathways, multiple bond frag-

mentations are required for neutral Fe and FeO loss. In the first step, a bridging Fe–O bond is broken and the oxygen either bonds to the Fe atom that is less coordinated requiring 0.59 eV or stays on the iron atom with another oxygen atom already attached requiring 0.90 eV of energy. At this stage in the reaction path, spin is conserved in the doublet state for the neutral FeO dissociation pathway. From the  $[\text{}^2\text{O}_2\text{FeOFeO}_2]$  transition state, the bonds are relaxed and followed by Fe–Fe dissociation to form a linear chain of alternating Fe–O bonds. Finally, neutral FeO

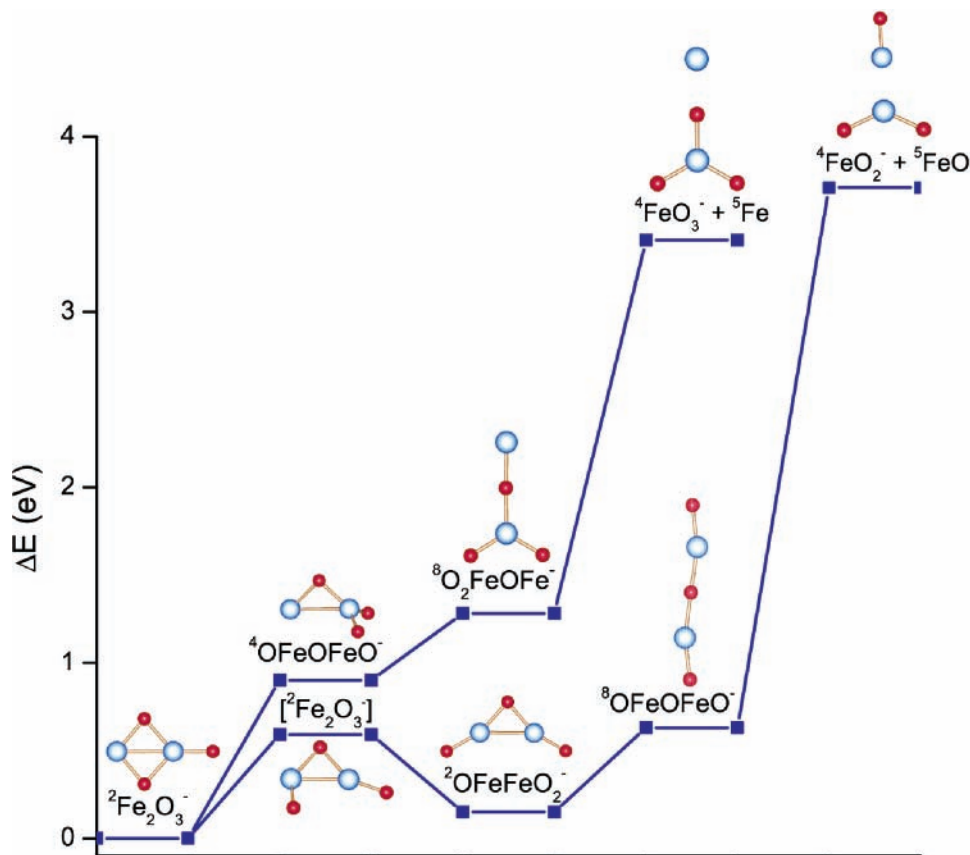


**Figure 7.** The change in energy ( $\Delta E$ ) for the dissociation pathway of  $\text{Fe}_2\text{O}_3^-$  to  $\text{FeO}_3^-$  and  $\text{FeO}_2^-$ . The superscripts indicate the spin multiplicity.

is released with an additional 3.08 eV of energy required. The other pathway for neutral Fe dissociation also requires a spin change and bond rearrangements. Subsequent neutral Fe loss from the cluster requires an additional 2.14 eV of energy.

While a comparison of the two pathways may indicate that the loss of Fe is energetically more favorable, the pathway for the loss of FeO involves more stable intermediate steps. We believe that this accounts for the FeO fragments being observed before Fe loss. Further, the numerous bond breaking steps and rearrangement of the atoms along the pathways may make these FeO and Fe loss mechanisms kinetically unfavorable compared to the energetically unfavorable O atom loss channel. In both cases (loss of FeO and loss of Fe), the need to undergo a spin transition from a doublet state to an octet intermediate state is expected to slow the reaction considerably.<sup>39</sup>

Additionally the calculated dissociation pathway for  $\text{Fe}_2\text{O}_6^-$ , which support our CID results, are provided in the Supporting Information (Figure S1, Table S5). For  $\text{Fe}_2\text{O}_6^-$  the fragmentation order observed with CID differs from the calculated dissociation energies. For the same reasons discussed above for  $\text{Fe}_2\text{O}_3^-$ ,  $\text{FeO}_3$  loss occurs after removal of an O atom. Multiple bond fragmentation in  $\text{Fe}_2\text{O}_6^-$  requires multiple collisions and therefore is observed after O atom loss.

**Reactions with CO and N<sub>2</sub>.** The reaction products for each cluster species are recorded in descending order of relative product intensity in Table 1. Theoretical studies indicate that the atomization energy of CO and CO<sub>2</sub> are 11.63 and 17.97 eV, respectively. The formation of CO<sub>2</sub> is, therefore, energetically feasible in cases where it takes less than 6.34 eV to remove an O atom from the cluster. However, the presence of reaction barriers can prevent the formation of CO<sub>2</sub>. This is the reason that CO<sub>2</sub> formation does not occur in the presence of O<sub>2</sub> even

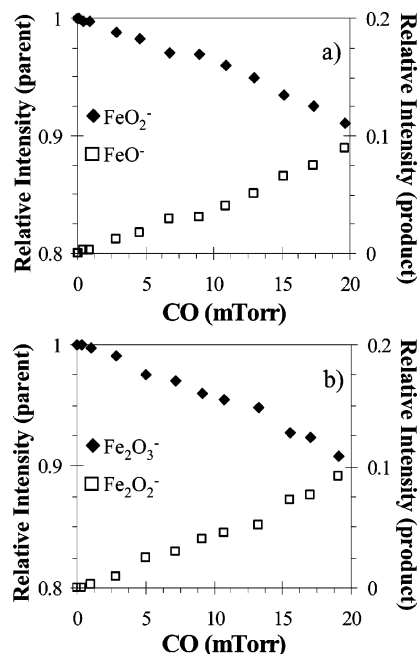


**Figure 8.** Relative intensities of (a)  $\text{FeO}_2^-$  and  $\text{FeO}^-$ , and (b)  $\text{Fe}_2\text{O}_3^-$  and  $\text{Fe}_2\text{O}_2^-$  as functions of CO reactant gas pressure. The observed behavior shows that both  $\text{FeO}_2^-$  and  $\text{Fe}_2\text{O}_3^-$  are effective for the oxygen atom transfer reaction.

though the binding energy of O<sub>2</sub> is only 6.20 eV. As Table 1 shows, the energy to remove an O from the cluster species,  $\text{FeO}_2^-$ ,  $\text{FeO}_3^-$ ,  $\text{FeO}_4^-$ ,  $\text{Fe}_2\text{O}_3^-$ ,  $\text{Fe}_2\text{O}_4^-$ , and  $\text{Fe}_2\text{O}_5^-$  is less than 6.34 eV, and they are all active toward oxygen atom transfer to CO. This process occurs as a dominant reaction channel for most anionic species. Since neutral species are not detected,

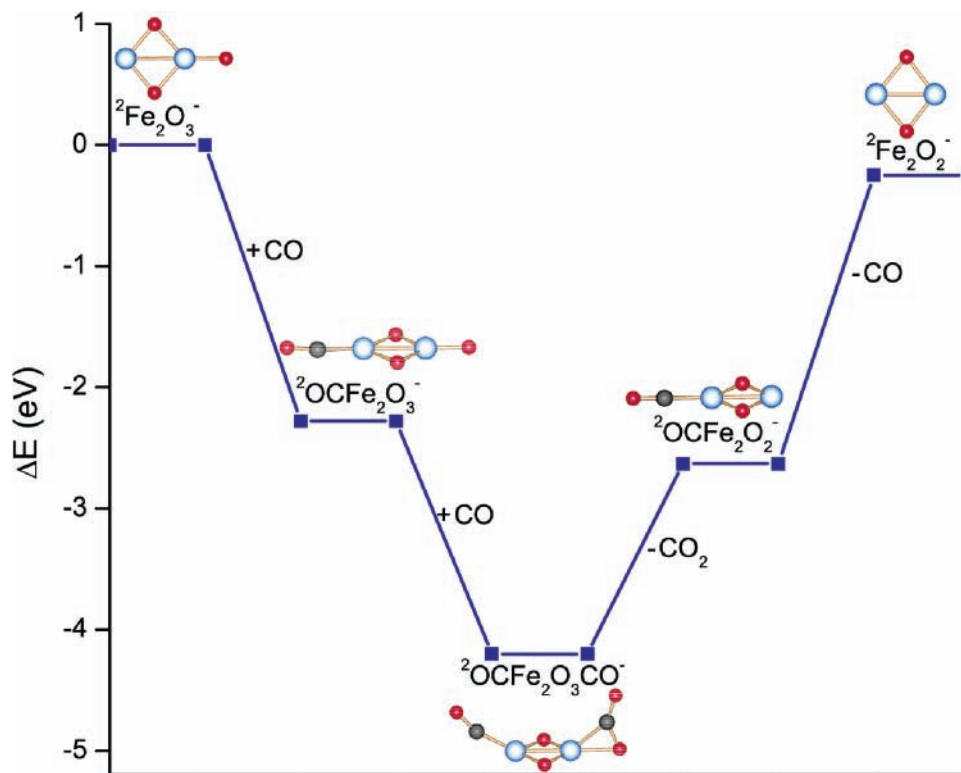


**Figure 9.** The change in energy ( $\Delta E$ ) for the reaction pathway of  $\text{Fe}_2\text{O}_3^-$  with CO. The superscripts indicate the spin multiplicity.

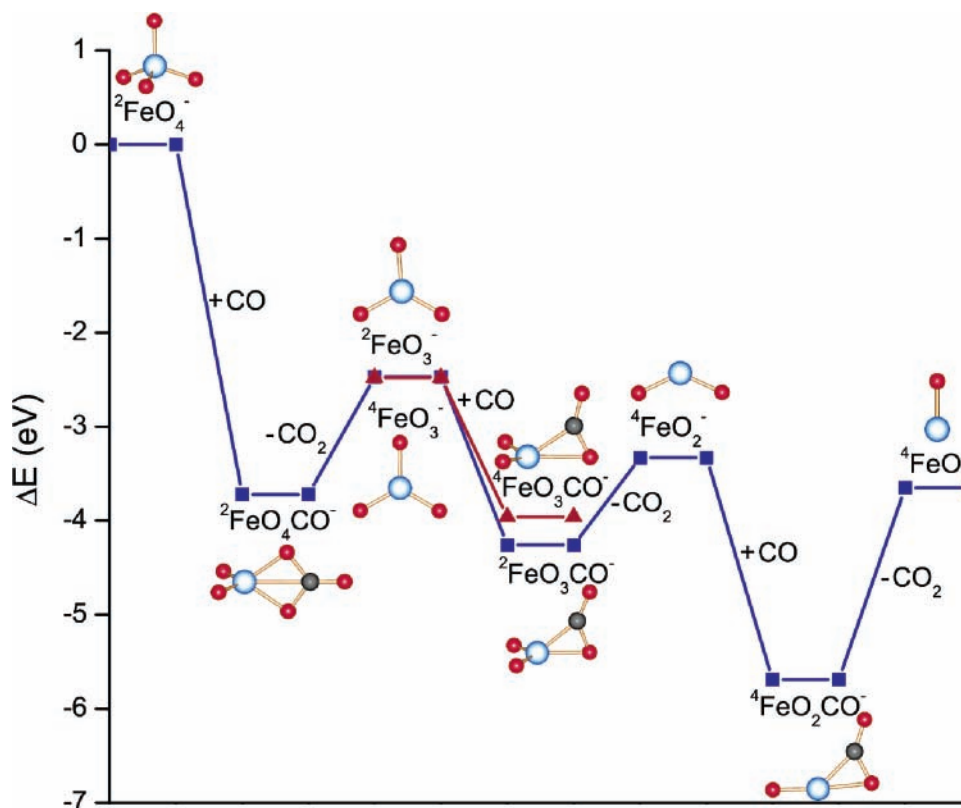


**Figure 10.** The change in energy ( $\Delta E$ ) for the reaction pathway of  $\text{FeO}_4^-$  with CO. The superscripts indicate the spin multiplicity.

the presence of  $\text{Fe}_x\text{O}_{y-1}^-$  products suggests that oxygen is transferred from iron oxide clusters to CO to produce neutral  $\text{CO}_2$ .

Figure 8 shows how the  $\text{FeO}_2^-$  and  $\text{Fe}_2\text{O}_3^-$  signals change as a function of increasing CO pressure. These cluster stoichiometries are the most efficient iron oxide anions to effect the CO oxidation reaction channel. Notice that both clusters are

composed of one more oxygen atom than the number of iron atoms. The energy calculated to remove an oxygen atom from these two clusters is approximately 6 eV. Therefore, the total energy needed is more than can be supplied through thermal collisions alone. This is supported by the fact that no oxygen atom loss products are observed in nitrogen studies conducted under the same experimental conditions (see Table 1). Confir-

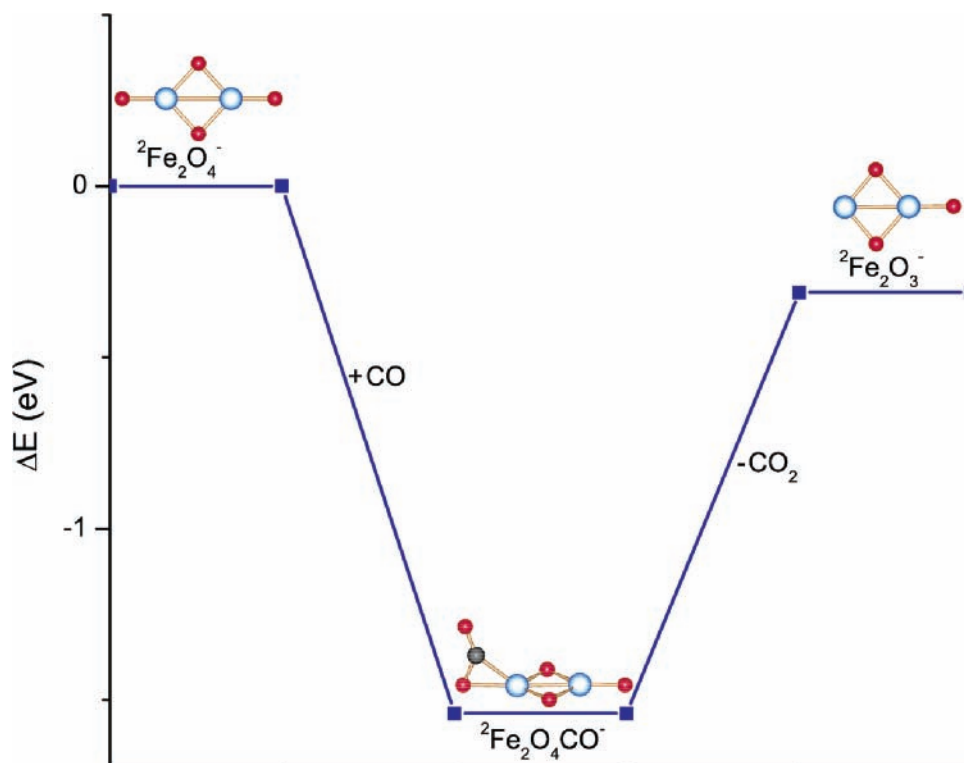


**Figure 11.** The change in energy ( $\Delta E$ ) for the reaction pathway of  $\text{Fe}_2\text{O}_4^-$  with CO. The superscripts indicate the spin multiplicity.

mation of the chemical reactivity of iron oxide anionic clusters with CO, therefore, can be seen by comparing the products to those observed with nitrogen.

We also calculated the reaction paths of the  $\text{FeO}_2^-$ ,  $\text{FeO}_3^-$ ,  $\text{FeO}_4^-$ ,  $\text{Fe}_2\text{O}_3^-$ , and  $\text{Fe}_2\text{O}_4^-$  clusters with CO in order to understand the different reactivity they displayed. We found that for the most active clusters,  $\text{FeO}_2^-$  and  $\text{Fe}_2\text{O}_3^-$ , the reaction proceeds without barriers and follows a spin allowed path. The reaction path for  $\text{Fe}_2\text{O}_3^-$  is shown in Figure 9 with the exact values provided in supplemental Table S6. The first CO can attach to the Fe site or approach the O atom to form  $\text{CO}_2$ . Our studies indicate that the more stable configuration corresponds to CO attached to the Fe site. This is consistent with the electron donating behavior of CO and the partial positive charge present on the Fe site, as revealed by the Mulliken population calculation. The subsequent CO then attaches to the O site forming  $\text{CO}_2$  as shown in Figure 9. Previous studies on neutral  $\text{Fe}_2\text{O}_3$  also obtained a similar reaction path.<sup>8</sup>

On the other hand, for  $\text{FeO}_4^-$  shown in Figure 10 and Table S7, the reaction with CO involves a change of spin which may slow the reaction. For the  $\text{Fe}_2\text{O}_4^-$  the reaction proceeds without barriers and follows a spin allowed path as revealed in Figure 11 and Table S8. In the initial step of the reaction, there is a gain in energy of only 1.54 eV for the absorption of the CO molecule compared with a gain of 4.20 eV for the absorption of two CO molecules in the  $\text{Fe}_2\text{O}_3^-$  cluster. This is because one of the Fe sites in  $\text{Fe}_2\text{O}_3^-$  is coordinated to only two O atoms and the first CO binds to this metal site. This difference in adsorption energy explains the difference in reactivity observed in the two clusters. It is important to note that the reaction pathways involve intermediate species and consequently require structural rearrangements. For small clusters, the reduced size is amenable to these rearrangements and consequently, the reaction barriers are far less than for the case of bulk surfaces where the extended geometry is less flexible toward structural changes.

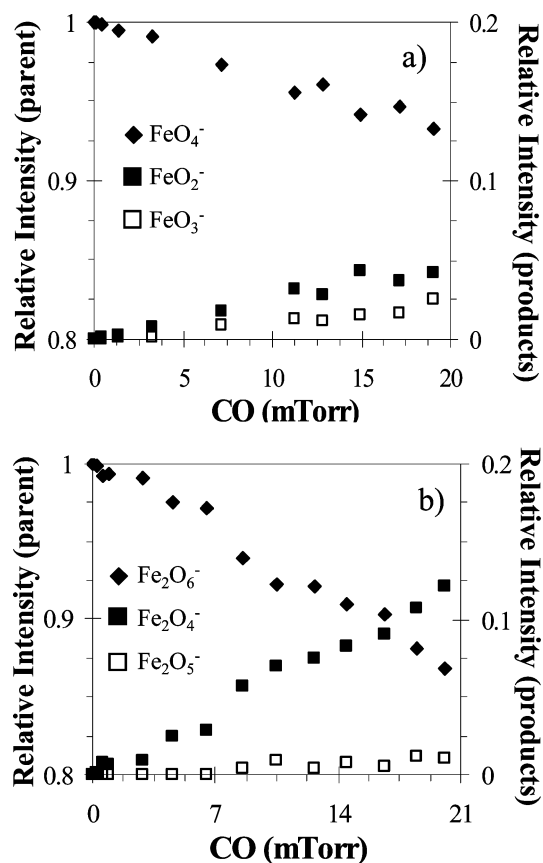


**Figure 12.** Relative intensities for (a)  $\text{FeO}_4^-$  and products species and (b)  $\text{Fe}_2\text{O}_6^-$  and product species as functions of increasing CO pressure. Notice both clusters show the dominant channel to be molecular oxygen loss over atomic oxygen loss.

Another reaction channel observed was the loss of molecular oxygen from  $\text{FeO}_4^-$  and  $\text{Fe}_2\text{O}_6^-$ . The change in cluster intensity with increasing CO pressure is shown in Figure 12, with  $\text{O}_2$

loss as the dominant reaction channel followed by minor O atom loss. In the case of  $\text{FeO}_4^-$ , it is presumed at the high CO pressures in which  $\text{FeO}_2^-$  is detected as a product, the loss of molecular oxygen can be attributed to collision excitation that promotes the cluster to the structure containing an intact molecular oxygen unit. The same will apply for the formation of the higher-energy isomer of  $\text{Fe}_2\text{O}_6^-$  with a molecular oxygen unit. Both  $\text{Fe}_2\text{O}_6^-$  and  $\text{FeO}_4^-$  showed  $\text{O}_2$  loss in the presence of nitrogen as seen in Table 1. These products were observed at higher nitrogen pressure under conditions where multiple collisions are expected.

## Conclusion

It is shown that the nature of fragments produced in collision induced dissociation is governed not only by the overall energetics but also by the nature and multiplicity of the intermediate states marking the fragmentation. For  $\text{FeO}_n^-$  clusters, the studies show that while the loss of atomic O is the favored channel at lower oxygen coverage, the loss of  $\text{O}_2$  becomes the dominant pathway when more oxygen surrounds a single Fe atom. In the case of  $\text{Fe}_2\text{O}_n^-$  clusters, the lowest-energy fragmentation pathways involve the loss of Fe or FeO units except for  $\text{Fe}_2\text{O}_6^-$ , where the lowest-energy pathway is the loss of an  $\text{O}_2$  molecule. Small anionic iron oxide clusters are shown to enable the oxidation of CO at near thermal energies. The most active and selective iron oxides were composed of one more oxygen atom than iron atom. The increased reactivity is attributed to two reasons. (1) The energy required to remove an O atom in these clusters is less than the gain in energy to form  $\text{CO}_2$  making the oxidation thermodynamically feasible. (2) The reduced size (compared to bulk species) allows structural rearrangements that eliminate/reduce the high reaction barriers and make the oxidation kinetically possible. We are in the process of extending these studies to cationic clusters and larger sizes to examine the effect of charge state and size on the catalytic conversion.

**Acknowledgment.** N.M.R., G.E.J., and A.W.C., Jr. gratefully acknowledge the U.S. Department of Energy, Grant No. DE-FG02-92ER14258, for financial support of the experimental work reported herein. J.U.R. and S.N.K. acknowledge support from U.S. Department of Energy Grant DE-FG02-02ER46009. S.N.K. is also grateful to VCU for providing a study/research leave.

**Supporting Information Available:** Tables with energies for dissociation pathways corresponding to figures described in the text; figure for the dissociation pathway for  $\text{Fe}_2\text{O}_6^-$  and corresponding energies; tables of energies for reaction pathways of figures in the text. This material is available free of charge via the Internet at <http://pubs.acs.org>.

## References and Notes

- (1) Li, X.-Q.; Zhang, W.-X. *Langmuir* **2006**, *22*, 4638.
- (2) Lin, H.-Y.; Chen, Y.-W.; Wang, W.-J. *J. Nanopart. Res.* **2005**, *7*, 249.
- (3) Yumura, T.; Amenomori, T.; Kagawa, Y.; Yoshizawa, K. *J. Phys. Chem. A* **2002**, *106*, 621.
- (4) Tanaka, S.; Nakagawa, K.; Kanezaki, E.; Katoh, M.; Murai, K.-I.; Moriga, T.; Nakabayashi, I.; Sugiyama, S.; Kidoguchi, Y.; Miwa, K. *J. Jpn. Pet. Inst.* **2005**, *48*, 223.
- (5) Schröder, D.; Schwarz, H.; Clemmer, D.; Chen, Y.; Armentrout, P. B.; Baranov, V. I.; Böhme, D. K. *Int. J. Mass Spectrom.* **1997**, *161*, 175.
- (6) Wu, K.-C.; Tung, Y.-L.; Chen, Y.-L.; Chen, Y.-W. *Appl. Catal., B* **2004**, *53*, 111.
- (7) Shiroishi, H.; Oda, T.; Hamada, I.; Fujima, N. *Eur. Phys. J. D* **2003**, *24*, 85.
- (8) Jones, N. O.; Reddy, B. V.; Rasouli, F.; Khanna, S. N. *Phys. Rev. B* **2005**, *72*, 165411.
- (9) Shiroishi, H.; Oda, T.; Hamada, I.; Fujima, N. *Polyhedron* **2005**, *24*, 2472.
- (10) Wu, H.; Desai, S. R.; Wang, L.-S. *J. Am. Chem. Soc.* **1996**, *118*, 5296.
- (11) Wang, L.-S. Photoionization and Photodetachment Part II. In *Advanced Series in Physical Chemistry*; Cheuk-Yiu, N., Ed.; World Scientific: River Edge, NJ 2000; Vol. 10B, pp 854–957.
- (12) Wang, L.-S.; Wu, H.; Desai, S. R. *Phys. Rev. Lett.* **1996**, *76*, 4853.
- (13) Li, P.; Miser, D. E.; Rabiei, S.; Yadav, R. T.; Hajaligol, M. R. *Appl. Catal. B* **2003**, *43*, 151.
- (14) Reddy, B. V.; Rasouli, F.; Hajaligol, M. R.; Khanna, S. N. *Fuel* **2004**, *83*, 1537.
- (15) Reddy, B. V.; Rasouli, F.; Hajaligol, M. R.; Khanna, S. N. *Chem. Phys. Lett.* **2004**, *384*, 242.
- (16) Reddy, B. V.; Khanna, S. N. *Phys. Rev. Lett.* **2004**, *93*, 068301.
- (17) Schubert, M. M.; Hackenberg, S.; van Veen, A. C.; Muhler, M.; Plzak, V.; Behm, R. J. *J. Catal.* **2001**, *197*, 113.
- (18) Kozlov, A. I.; Kozlova, A. P.; Liu, H.; Iwasawa, Y. *Appl. Catal. A* **1999**, *182*, 9.
- (19) Lin, H.-Y.; Chen, Y.-W. *Ind. Eng. Chem. Res.* **2005**, *44*, 4569.
- (20) Fialko, E. F.; Kikhtenko, A. V.; Goncharov, V. B.; Zamaraev, K. I. *J. Phys. Chem. B* **1997**, *101*, 5772.
- (21) Witko, M.; Hermann, K.; Tokarz, R. *J. Electron. Spec. Relat. Phenom.* **1994**, *69*, 89.
- (22) Muetterties, E. L. *Science* **1997**, *196*, 839.
- (23) Somorjai, G. A. *Introduction to Surface Chemistry and Catalysis*; John Wiley: New York, 1994; pp 402–409.
- (24) Zemski, K. A.; Justes, D. R.; Castleman, A. W., Jr. *J. Phys. Chem. B* **2002**, *106*, 6136.
- (25) Reilly, N. M.; Johnson, G. E.; Castleman, A. W., Jr.; Reveles, J. U.; Khanna, S. N. Experimental and Theoretical Study of the Structures and Reactivity of  $\text{Fe}_{1-2}\text{O}_{1-5}^+$  with CO. Manuscript in preparation.
- (26) Bell, R. C.; Zemski, K. A.; Justes, D. R.; Castleman, A. W., Jr. *J. Chem. Phys.* **2001**, *114*, 798.
- (27) Kohn, W.; Sham, L. J. *Phys. Rev.* **1965**, *140*, A1133.
- (28) Perdew, J. P.; Burke, K.; Ernzerhof, M. *Phys. Rev. Lett.* **1996**, *77*, 3865.
- (29) Pederson, M. R.; Jackson, K. A. *Phys. Rev. B* **1990**, *41*, 7453.
- (30) Jackson, K.; Pederson, M. R. *Phys. Rev. B* **1990**, *42*, 3276.
- (31) Porezag, D.; Pederson, M. R. *Phys. Rev. A* **1999**, *60*, 2840.
- (32) Köster, A. M.; Calaminici, P.; Casida, M. E.; Flores-Moreno, R.; Geudtner, G.; Goursot, A.; Heine, T.; Ipatov, A.; Janetzko, F.; del Campo, M. J.; Patchkovskii, S.; Reveles, J. U.; Vela, A.; Salahub, D. R. *deMon2k*, version 2.2.6; International deMon Developers Community: 2006. <http://www.deMon-software.com>; Köster, A. M.; Flores-Moreno, R.; Reveles, J. U. *J. Chem. Phys.* **2004**, *121*, 681; Reveles, J. U.; Köster, A. M. *J. Comput. Chem.* **2005**, *25*, 1109.
- (33) Godbout, N.; Salahub, D. R.; Andzelm, J.; Wimmer, E. *Can. J. Chem.* **1992**, *70*, 560.
- (34) Wachters, A. J. H. *J. Chem. Phys.* **1970**, *52*, 1033; *IBM Tech. Rep.* **1969**, RJ584. For *F* exponents, see: Bauschlicher, C. W., Jr.; Langhoff, S. R.; Barnes, L. A. *J. Chem. Phys.* **1989**, *91*, 2399.
- (35) Shin, D. N.; Matsuda, Y.; Bernstein, E. R. *J. Chem. Phys.* **2004**, *120*, 4150.
- (36) Reddy, B. V.; Khanna, S. N. *Phys. Rev. Lett.* **1999**, *83*, 3170.
- (37) Bell, R. C.; Zemski, K. A.; Kerns, K. P.; Deng, H. T.; Castleman, A. W., Jr. *J. Phys. Chem. A* **1998**, *102*, 1733.
- (38) Justes, D. R.; Mitrić, R.; Moore, N. A.; Bonačić-Koutecký, V.; Castleman, A. W., Jr. *J. Am. Chem. Soc.* **2003**, *125*, 6289.
- (39) Schwarz, H. *Int. J. Mass Spectrom.* **2004**, *237*, 75.